Pore fluid and porosity mapping from seismic

Jack Dvorkin and Salman Alkhater*

Abstract

We use rock physics to map pore fluid and porosity from seismic data in a vertical section between two wells. First, well log data are used to establish an effective-medium model that links the impedance to pore fluid and porosity. Next, stacked seismic data are used to produce P-wave impedance inversion. Finally, the rock physics transform is applied to the impedance section to identify pore fluid and produce a porosity section.

Introduction

For decades, the main use of seismic data has been to delineate sedimentary bodies and tectonic features in the subsurface. The mission of exploring *inside* the geological body is a relatively recent development. Mapping porosity, lithology and other reservoir bulk properties inside the geological body has become possible due to the recent dramatic improvement in seismic acquisition, imaging and inversion quality, as well as the accompanying advances in rock physics.

Rock physics provides transforms between a reservoir's elastic properties and its bulk properties and conditions, including porosity, lithology, pore fluid and pore pressure. Such transforms are known as *trends*. Trends are built from controlled experiments where both the elastic and bulk properties of rock are measured on the same samples under the same conditions. The most commonly used source of such experimental data in modern rock physics is the borehole measurement. For example, an empirical impedance–porosity trend developed from sonic, density and porosity curves can be applied to a seismic acoustic impedance volume in order to map porosity in 3D.

However, it is always advantageous not only to find an empirical trend but also to understand the physical laws that determine the trend or, in other words, find an appropriate effective-medium model. Such *rationalization* of an empirical trend by effective-medium modelling generalizes the trend, determines the domains of its applicability, and thus reduces the risk of using the trend outside the immediate data range.

Here, we illustrate the rational-rock-physics approach by mapping porosity in a large producing gas/oil reservoir. Well data are used to establish a transform from impedance to porosity, based on rock-physics theory. This transform is then applied to a vertical impedance section obtained from stacked seismic data via inversion.

The reservoir under examination consists of relatively soft sands. As a result, the acoustic impedance of the gas-saturated sand is much lower than that of the oil- and water-saturated sand. This large impedance difference allows us to

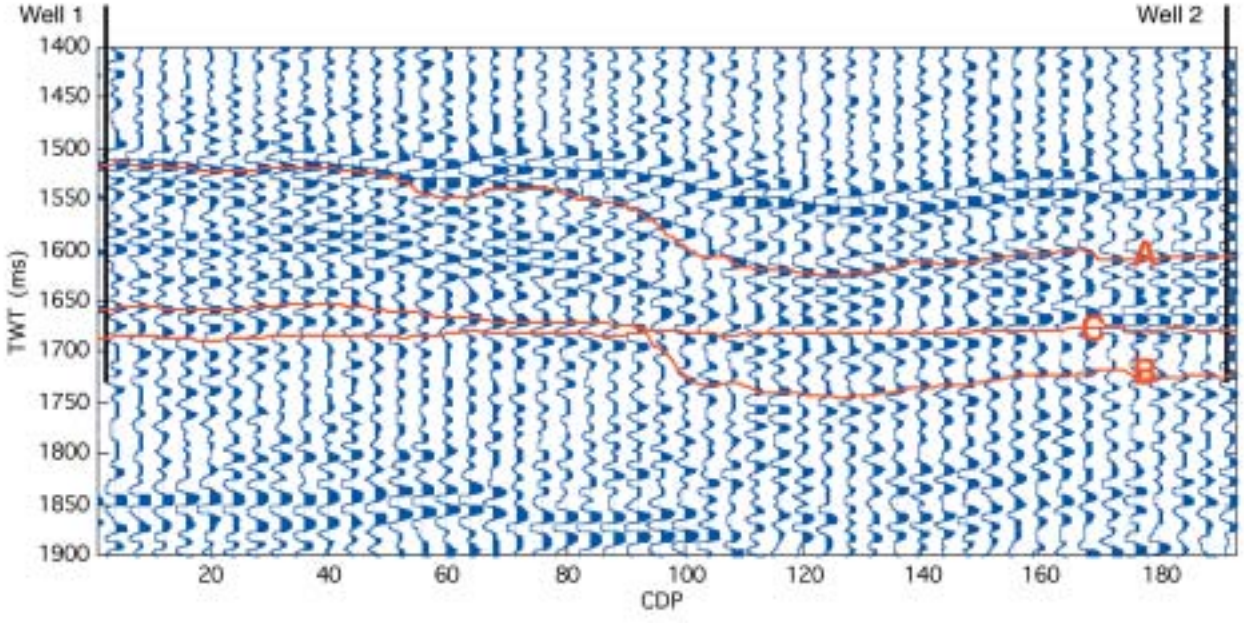

Figure 1 *The seismic section (full stack) between two vertical wells. The reservoir is located between reflectors A and B. Reflector C marks the transition from gas to oil.*

* *Stanford Rock Physics Laboratory*

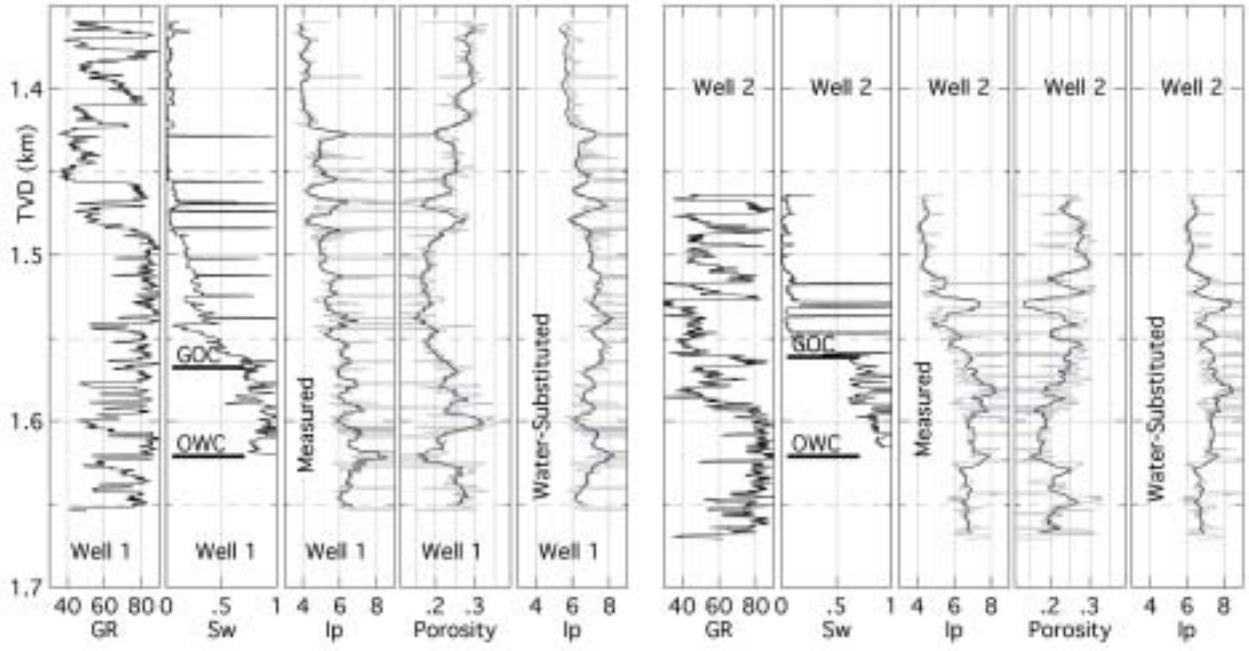

Figure 2 *Well-log data for Well 1 (left) and Well 2 (right). The well-log curves are (from left to right): gamma-ray (API); hydrocarbon saturation (fraction); measured P-wave impedance (km/s g/cc); total porosity (fraction); P-wave impedance (km/s g/cc) calculated for 100% water saturation. The porosity and impedance frames also show the upscaled curves that are the running mean average for porosity and the Backus average for impedance with one-quarter wavelength used as an averaging window.*

identify the pore fluid from P-wave data only, without using offset information. As a result, we map both pore fluid and porosity, using only stacked seismic data.

Seismic data

The seismic line under examination (Fig. 1) connects two vertical wells and was extracted from a 3D seismic volume in the North Sea Troll Field. The data were sampled at 2 ms intervals and stacked at all offsets. The two wells are located at CDP gathers 3 and 190. The two-way traveltime window of interest is between 1400 and 1900 ms. The reservoir is located between two seismic horizons (A and B in Fig. 1). The gas–oil contact is located at the flat reflector C. The relief of the reservoir changes abruptly in the middle of the section, which is typical for the step-like offshore sediment topology in the Troll Field.

Well-log data and rock-physics diagnostics

Both the wells that bound the seismic line are producers and they penetrate an extensive gas cap and the underlying oil and water intervals (see well-log curves in Fig. 2). The intervals in both wells are dominated by very high-impedance and low-porosity calcite-cemented layers. These layers are likely to affect the seismic response of the reservoir significantly.

The pore-fluid system in the reservoir includes gas, oil and water. We assume that there is only gas and water above the gas–oil contact and only oil and water between the gas–oil and oil–water contacts. In other words, gas and oil do not coexist in the reservoir.

The *in situ* physical properties of the reservoir fluids, as calculated from gas and oil gravity, gas-to-oil ratio, water salinity, and pressure and temperature using the Batzle and Wang (1992) relationships, are summarized in Table 1.

To develop an impedance–porosity transform, we first bring the data to the *common fluid denominator*, i.e. calculate the P-wave impedance in both wells for 100% water saturation using the P-wave-only fluid-substitution method of Mavko *et al.* (1995). This method replaces the traditional Gassmann's (1951) fluid substitution where shear-wave data are not available.

The water-substituted impedance curves are also displayed in Fig. 2. These curves practically mirror-image the total porosity curves in both wells, which implies the existence of an impedance–porosity trend. The impedance–porosity crossplots show that these trends do exist (Fig. 3). They are especially clear in the gas-cap intervals of both wells.

Fluid Type	Density (g/cc)	Bulk Modulus (GPa)
Gas	0.122	0.031
Oil	0.695	0.664
Water	1.034	2.71

Table 1 *Physical properties of gas, oil and water used in the study*

In order to describe the impedance–porosity trends shown in Fig. 3, we use the uncemented sand model of Dvorkin & Nur (1996) and the constant cement model of Avseth *et al*. (2000). The red curves in the impedance–porosity crossplots in Fig. 3 are from the first model for sand with clay content of 0%, 10% and 20%. The black curves are from the constant-cement model.

By drawing the effective-medium curves, we are able to identify two principal branches in the data. The first branch is comprised of high-porosity relatively stiff sands that have very small amounts of contact quartz cement (the black model line in Fig. 3). The second branch is comprised of uncemented sands with very small amounts of clay. This trend separation is also common in the Troll Field and is determined by grain sorting. Large well-sorted grains may have small quantities of cement covering them while the presence of even a small amount of clay inhibits cement formation (Avseth *et al*. 2000).

We conclude that the impedance–porosity behaviour in the reservoir under examination can be accurately described by both the uncemented and the slightly cemented sand models, depending on the type of sand.

Upscaling

The seismic wavelength is usually much larger than the scale of rock-property variation observed in well-log data. Let us assume that the average P-wave velocity is 2.5 km/s and the dominant frequency is 50 Hz. Then the wavelength is 50 m and the quarter-wavelength is 12.5 m. In order to understand how the rock properties observed from seismic are related to those derived from well logs and also how the rock-physics transforms relevant to well-log data hold at the seismic scale, we conduct upscaling using the quarter-wavelength as an averaging window.

The two rock properties to be linked to each other are (a) the total porosity and (b) the P-wave impedance. Therefore, for both wells, we (a) calculate the average porosity by applying the running mean filter to the data and (b) calculate the effective impedance by using the Backus (1962) average. These mean porosity and effective impedance curves are displayed in Fig. 2, together with the log-scale measurements. The effective (fluid-substituted) impedance is crossplotted versus the average porosity in Fig. 3, next to the log-scale crossplots.

The upscaled crossplots appear to be even tighter than the log-scale crossplots, especially in the gas zone of Well 1. After upscaling, the data points move from the constant cement line on to the clean uncemented sand line, most probably due to the effects of the Backus averaging on the impedance (the Backus average is the geometric average of the compressional moduli and as such gives more weight to the softest layers in the sequence (G. Mavko, pers. comm.)).

The upscaled data lie between the 0% clay and 20% clay uncemented sand lines. This spread determines the accuracy of porosity determination from seismic (about ±0.03 porosity units).

Identifying pore fluid

In the soft sand under examination, the effect of pore fluid on the P-wave impedance is so large that it allows us to discriminate the gas-saturated sands from the liquid-saturated sands by using simple impedance cut-off. Consider Fig. 4 (left) where the upscaled impedance is plotted versus the upscaled total porosity for both wells and colour-coded according to the pore fluid.

The impedance in the gas cap (red symbols) predominantly lies below 6 km/s g/cc while the impedance of the oil- and water-saturated intervals lies above the 6 km/s g/cc mark. This clear cut-off allows us to identify the pore fluid from P-wave data by following a simple rule, i.e. gas is present where the P-wave impedance is lower than 6 km/s g/cc and oil or water is present where it is higher than 6 km/s g/cc. Note that this cut-off is not universal. It is valid for the soft sand under examination and is field and facies specific.

Transform from impedance to porosity

In order to derive porosity from impedance, we use the transform given by the uncemented sand model for 10% clay content that describes, on average, the trends present in the data

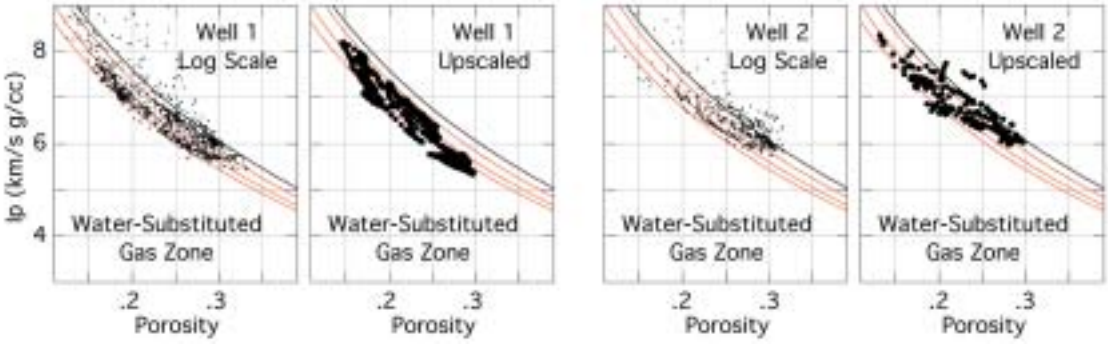

Figure 3 *Impedance–porosity crossplots of water-substituted well-log data at the original log scale as well as upscaled. The curves in the crossplots are from effective-medium models. The red curves are from the uncemented sand model with clay content of 0%, 10% and 20%. The black curve is from the constant cement model. In the models, the critical porosity is 0.4, the coordination number is 8 and the cemented porosity is 0.375.*

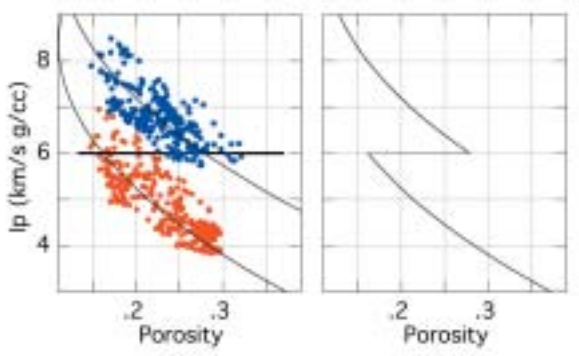

Figure 4 *Left: Upscaled impedance versus upscaled total porosity in both wells. The red symbols come from the gas cap while the blue symbols are from the oil/water zone. The horizontal bar is the cut-off used for pore-fluid identification. The curves are given by the uncemented sand model for 10% clay content, for water (top) and gas (bottom). Right: Impedance to porosity transform as given by equations (1) and (2) and the cut-off between the gas- and liquid-saturated intervals.*

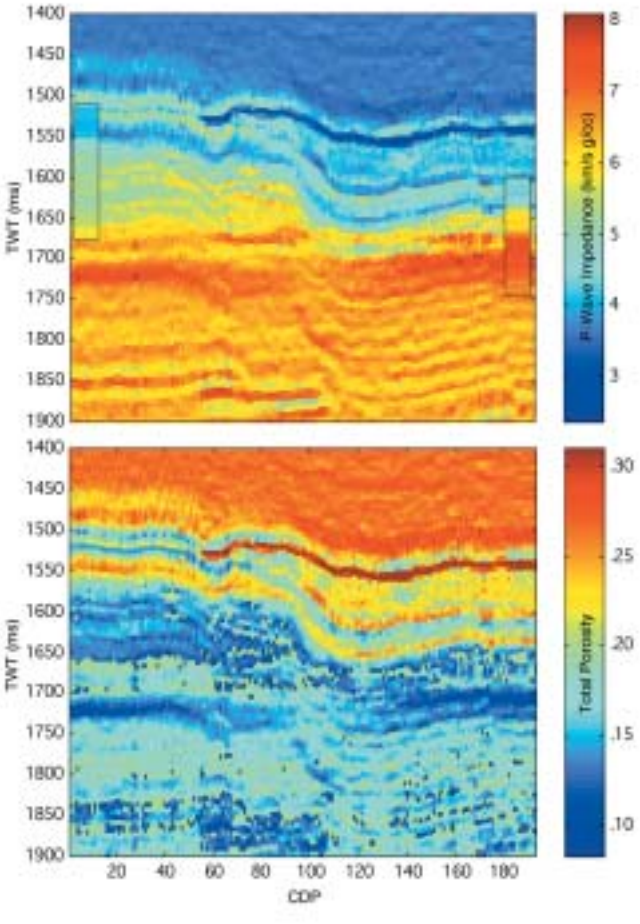

Figure 5 *Impedance inversion section (top) and predicted porosity section (bottom).The inserted strips in the upper frame mark the impedence in the wells*

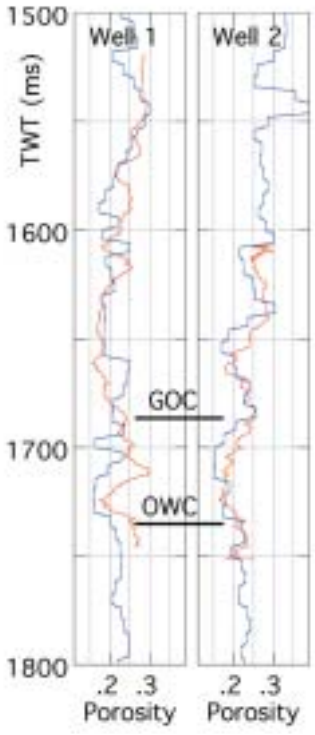

Figure 6 *Porosity from seismic (blue) and upscaled porosity from well logs (red) versus two-way traveltime for Well 1 (left) and Well 2 (right). The horizontal bars mark the gas–oil and oil–water contacts.*

(Fig. 4, left). The exact model equations are algebraically involved and therefore it is inconvenient to apply these equations to the seismic impedance inversion data directly. We simplify these transforms by least-squares polynomial fitting.

The resulting equations are

$$\phi = 0.744 - 0.515I_P + 0.009I_P^2 \quad (1)$$

for $I_P < 6$ (gas cap), and

$$\phi = 1.065 - 0.185I_P + 0.009I_P^2 \quad (2)$$

for $I_P \geq 6$ (oil/water zone).

These equations, combined with the 6 km/s g/cc cut-off, are plotted in Fig. 4 (right).

Impedance inversion and porosity mapping

To obtain a porosity map using equations (1) and (2), we first conduct impedance inversion on the fully stacked seismic data using the Hampson–Russell STRATA inversion package. The impedance inversion section is shown in Fig. 5 (top). As expected, the seismic impedance closely matches the impedance in the wells. In this section, we can clearly identify the two horizons that bound the reservoir as well as

the flat reflector that marks the gas–oil contact. The impedance dramatically increases across this contact.

Next we apply the impedance–porosity transform functions, given by equations (1) and (2), to the impedance section. The resulting total porosity section is shown in Fig. 5 (bottom). The predicted porosity curves at the wells are compared to the upscaled well-log data in Fig. 6. The seismic porosity curves closely track the upscaled well-log porosity curves. The mismatch present in some sections of Well 1 is probably due to the scatter of data around the impedance–porosity transform curves (Fig. 4).

Note that the porosity section is qualitatively different from the impedance section, i.e. it does not reflect the sharp horizontal impedance contrast at the flat gas–oil contact reflector (about 1680 ms two-way traveltime). This is because before using the impedance–porosity transforms, we identified the pore fluid and then applied the transforms selectively, according to equations (1) and (2).

Conclusion

Model-based rock physics analysis of well-log data combined with seismic impedance inversion allows us to see inside a reservoir and, by producing reservoir property volumes, to go beyond outlining geobodies and mapping lithofacies. In the framework of this approach, it is paramount to understand the factors that affect the trends present in the data and to describe these trends by an effective-medium model rather than by a direct statistical fit.

We have shown that, in soft sand, it is possible to discriminate gas-saturated intervals from liquid-saturated intervals by using only P-wave data. This result, however, does not eliminate the need for AVO analysis as the primary tool for hydrocarbon detection. The reason is that in certain environments, water-saturated shale may be as soft as gas-saturated sand and the latter can only be delineated on the basis of a low Poisson's ratio.

The resolution of reservoir properties produced by integrating rock physics and seismic still does not exceed seismic resolution. As a result, it should not be expected that, without additional stringent assumptions, reservoir properties can be mapped at sub-seismic resolution. By using the deterministic approach described here, we only can image average properties, such as average porosity.

Acknowledgements

The data and technical advice, as well as part of the funding for this study, were supplied by Norsk Hydro. This study was also supported by the Stanford Rock Physics Laboratory and Saudi Aramco.

References

Avseth, P., Dvorkin, J., Mavko, G. and Rykkje, J. [2000] Rock physics diagnostic of North Sea sands: Link between microstructure and seismic properties. *Geophysical Research Letters* **27**, 2761–2764.

Backus, G.E. [1962] Long-wave elastic anisotropy produced by horizontal layering. *Journal of Geophysical Research* **67**, 4427–4440.

Batzle, M. and Wang, Z. [1992] Seismic properties of pore fluids. *Geophysics* **57**, 1396–1408.

Dvorkin, J. and Nur, A. [1996] Elasticity of high-porosity sandstones: Theory for two North Sea datasets. *Geophysics* **61**, 1363–1370.

Gassmann, F. [1951] Über die Elastizität poröser medien. *Vier. Der Natur. Gesellschaft in Zürich* **96**, 1–23.

Mavko, G., Chan, C. and Mukerji, T. [1995] Fluid substitution: Estimating changes in Vp without knowing Vs. *Geophysics* **60**, 1750–1755.

